Soft Matter

Effect of side-chain length on solute encapsulation by amphiphilic heterografted brush copolymers

Journal:	*Soft Matter*
Manuscript ID	SM-ART-06-2020-001190.R2
Article Type:	Paper
Date Submitted by the Author:	08-Aug-2020
Complete List of Authors:	Garcia, Elena; Colorado State University, Chemical and Biological Engineering Luo, Hanying; MilliporeSigma Milwaukee Mack, Courtney; Colorado State University, Chemical and Biological Engineering Herrera-Alonso, Margarita; Colorado State University, Chemical and Biological Engineering

ARTICLE

Effect of side-chain length on solute encapsulation by amphiphilic heterografted brush copolymers

Received 00th January 20xx,
Accepted 00th January 20xx

DOI: 10.1039/x0xx00000x

Elena A. Garcia,[a] Hanying Luo,[b] Courtney E. Mack [a] and Margarita Herrera-Alonso[a]†

Anisotropic nanomaterials are non-spherical structures that possess unique shape-dependent physicochemical properties and functionalities. Inspired by the abundance of filamentous entities in nature, cylindrical nanostructures have gained significant attention due to their unique performance. Herein, we discuss the effect of side-chain length on the encapsulation properties of amphiphilic heterografted bottlebrushes. We observed that by grafting a long hydrophilic block to the double-brush, we were able to restrict solute-induced conformational changes, thus producing drug-loaded anisotropic carriers. Unimolecular encapsulation in brushes was solute-dependent as shown here for probucol and rose bengal lactone. Stabilization with an amphiphilic diblock copolymer —consisting of the same type of blocks as those comprising the heterografted brush— served to explain the solute-dependent behavior observed for brushes, suggesting that solutes with a higher propensity to nucleation could be more effectively stabilized by the anisotropic carrier in a unimolecular worm-like construct.

Introduction

Anisotropic nanomaterials are non-spherical structures that possess unique shape-dependent physicochemical properties and functionalities. Although spherical nanoparticles are most commonly used for biomedical delivery applications, primarily due to their ease of fabrication, there has been growing interest in the study of how materials of different shapes (*e.g.*, rods, disks, stars, cubes) interact with biological systems.[1] Inspired by the abundance of filamentous entities in nature (*e.g.*, filoviruses, bacilli, E. Coli, collagen), cylindrical nanostructures have gained significant attention due to their superior performance compared to spherical nanoparticles.[2] The elongated geometry of cylindrical structures accounts for their large surface area compared to spheres,[3] where such expanded morphology results in higher drug encapsulation capacity.[4] Some of the other well-known advantages of cylindrical nanopartices include prolonged circulation time, reduced rate of clearance and non-specific cellular uptake, and enhanced active targeting.[1-6] Whereas not too long ago, nanostructures of complex morphologies were just a theoretical concept, recent advances in both polymerization techniques and self-assembly strategies have allowed the fabrication of particles with well-defined shape and size.

Polymeric micelles from amphiphilic polymers have been extensively studied for the delivery of poorly water-soluble compounds. Their hydrophobic micellar core not only provides the solutes protection from the environment, but also solubilizes these compounds through hydrophobic interaction. While polymer micelles have shown significant advantages over small-molecule analogs, they have also been reported to suffer from disruption or dissociation caused by dilution in the bloodstream, the effects of large shear forces on circulation, and/or interaction with serum proteins. These effects reduce the therapeutic efficacy of encapsulated drugs by leading to premature drug leaching, and ultimately may result in systemic toxicity. One strategy to address instability issues of polymeric nanoparticles includes the use of unimolecular micelles.[7] Common examples of unimolecular micelles include cyclic polymers,[8, 9] dendrimers,[10, 11] hyperbranched polymers,[12, 13] and multi-arm star-like polymers.[14-17] In recent years, however, alternative polymer architectures have started gaining importance as unimolecular carriers; these include bottlebrush polymers and grafted copolymers.[18-21]

Macromolecular brushes or bottlebrush polymers are a particular class of graft copolymers in which graft spacing — the size of the segments separating grafting points— is shorter than the side-chain length. Their architectural complexity translates into intramolecular excluded volume effects that cause long backbones to adopt a preferred cylindrical shape with radially emanating side-chains. Bottlebrushes can be rendered amphiphilic by grafting hydrophobic and hydrophilic segments onto the backbone.[22-27] Under conditions of poor solvent quality, and depending on polymer structure (*i.e.*,

[a] *Department of Chemical and Biological Engineering, School of Advanced Materials Discovery, Colorado State University, Fort Collins, Colorado 80523.*
[b] *Current address: Millipore Sigma, Sigma-Aldrich Corp. 6000 N. Teutonia Av. Milwaukee, Wisconsin 53209.*
† To whom the correspondence should be addressed.
Electronic Supplementary Information (ESI) available: The experimental section includes protocols for polymer synthesis and characterization, as well as NMR data of polymers, SANS data, static light scattering results and drug loading capacity and efficiency results. See DOI: 10.1039/x0xx00000x

backbone length, side chain length, graft spacing, and monomer sequence), the solvophobically-induced intrachain organization of graft or brush copolymers can result in spherical, 'pearl necklace-like,' or cylindrical aggregates.[28, 29] The types of bottlebrushes most commonly used for delivery purposes are those with a pre-assembled micellar character,[30-32] and the drug of interest can be loaded either through a covalent attachment or hydrophobic/ionic interactions.[7, 33-36] Yet another class of multi-component brushes are the heterografted type wherein two different blocks are attached at the block junction in a double-brush architecture.[31, 37-40] These have been explored as Janus nanomaterials and stabilizers of biphasic systems.[41-43] Molecular dynamics simulations have also been used to explore the roles of structural parameters and degree of side-chain incompatibility on their self-assembly triggered by a rapid quench in solvent quality.[44]

We have previously reported on the use of amphiphilic heterografted brushes consisting of a poly(glycidyl methacryalte) backbone with poly(D,L-lactide) and poly(ethylene glycol) side-chains ($PGMA_{721}$-*g*-PEG_{45}/PLA_{15}) for the encapsulation of hydrophobic solutes. The copolymer, which in water exhibited a worm-like structure consistent with an extended backbone conformation, collapsed into spherical particles in the presence of the solutes due to core-compaction.[20] In contrast, Zhou *et al.*, studied the encapsulation of doxorubicin in amphiphilic bottlebrushes and observed no conformational changes to the brush on encapsulation.[45] As Chen *et al.* have shown, morphological transitions of amphiphilic bottlebrushes are dependent on side-chain length and shell branching, as studied for bottlebrushes containing either linear or toothbrush-like hydrophilic side-chains.[46] Their findings showed that brushes with a comb-like side-chains retained their cylindrical shape upon solvent-induced collapse, in contrast to brushes with linear side-chains, which underwent a worm-to-sphere transition and were easily prone to intermolecular aggregation.

To fully realize the potential of bottlebrushes as anisotropic drug carriers, it is necessary to understand the role of hydrophilic side-chain length on their morphologies in the presence of guest molecules. Herein, we examine the encapsulation of hydrophobic solutes in heterografted bottlebrushes with comparatively longer hydrophilic side-chains than in our previous study[20] to understand the solute-triggered conformational changes of this class of amphiphilic polymer. Our observations regarding encapsulation in heterografted brushes will also be discussed in the context of stabilization with linear diblock copolymers to explain solute-specific behavior.

Experimental

Details regarding materials synthesis and characterization are provided in the Supporting Information.

Results and Discussion

Heterografted amphiphilic double-brushes consisting a poly(glycidyl methacryalte) backbone with poly(D,L-lactide) and poly(ethylene glycol) side-chains ($PGMA_{721}$-*g*-PEG_{45}/PLA_{15}) were previously shown to effectively stabilize hydrophobic solutes by undergoing a conformational worm-to-sphere transition in response to the solutes and a change in solvent quality of the medium. At low solute concentrations (feed composition of 5-15% $w_{solute}/w_{polymer}$, or mass of solute per mass of polymer), brushes collapsed unimolecularly into single-bottlebrush spherical nanoparticles with high encapsulation efficiency. As the solute content increased (20-100% $w_{solute}/w_{polymer}$), single-bottlebrush nanoparticles were no longer present, instead larger polydisperse aggregates were observed.[20]

To evaluate the effect of hydrophilic side-chain length on the solute-induced conformational transitions of heterografted brushes, we synthesized amphiphilic double brushes with comparatively longer PEG grafts than those previously discussed (5 kDa vs. 2 kDa) and examined their extent of loading and associated solute-induced morphological changes. The structure of the amphiphilic double brush (**B2**) is shown in **Figure 1**, and details regarding its synthesis are provided as Supplementary Information. A representative electron micrograph of the copolymer (**Figure 1**) shows it exhibits a worm-like morphology. The presence of smaller particles is believed to result from the interaction of the brush with the underlying grid, since backbone polydispersity was very low for this sample ($Đ$=1.14). Statistical analysis of this and other TEM images yielded average brush lengths and widths of 233 nm and 23 nm, respectively. The average length is reasonable as it falls between the theoretical brush contour length, assuming the backbone is in its fully extended conformation, and the side-chains are between their fully extended and Flory states.[20] Brush width, shows that the PEG chains along the length of the backbone not highly extended (R_f = 6 nm for PEG 5k), which would yield a theoretical width of 24 nm.

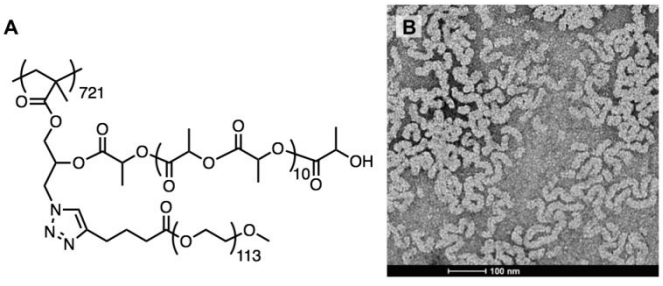

Figure 1. (**A**) Structure of heterografted PEG/PLA double-brush **B2**. (**B**) TEM image of **B2** cast from dimethylformamide. The sample was dissolved in the solvent (0.03 wt %) and cast directly onto carbon-coated TEM grids. Brush morphology can be described primarily as worm-like. Statistical analysis from this and other images yielded an average brush length of 233 nm and a width of 23 nm.

Brush morphology in solution was examined by small-angle neutron scattering. SANS experiments were performed at ambient temperature on the NG-7 30 m SANS instrument at the National Institute of Standards and Technology, Center for Neutron Research. An incident wavelength of 6.0 Å was used with sample-detector distances of 1, 4 and 13 m to cover a q-range from 0.003 to 0.55 $Å^{-1}$. Depending on backbone length, this range provides information regarding the overall size of the polymer (low q-range) and a measure of its stiffness and cross-sectional dimensions (intermediate q-range). Brush morphology was examined in three different solvents (*d*-DMSO, *d*-DMF and *d*-THF, 1 mg/mL), yielding similar scattering profiles (**Figure 2, A and S4**). While it was not possible to observe the low-q region given the length of the brush (> 200 nm), SANS data provided important information regarding brush cross-section.[47-49] A Guinier-Porod analysis of the data in DMSO yielded a dimension parameter of s = 0.72 and a cross-sectional radius of gyration of $R_{g,cs}$=6.7 nm. The radius of gyration of the cross-section can be used to estimate the radius of the brush as $R = R_{g,cs}\sqrt{2}$,[47] to give R = 9.5 nm. Brush diameter, estimated from SANS ($2R$ = 19 nm), has a similar value to brush width measured by TEM (23 nm), and their discrepancy may be attributed to a combination of drying effects or surface interaction with the underlying grid in TEM. Finally, the form factor in the intermediate-q range had a $1/Q^{1.0}$ dependence, indicative of a stiff cylinder with a finite radius.[50, 51] Similar results were obtained from scattering profiles of the polymer in *d*-DMF and *d*-THF (**S4**).

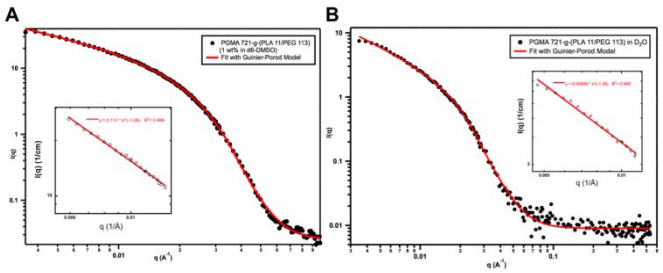

Figure 2. Small-angle neutron scattering profiles of **B2** double-bottlebrushes in DMSO-d_6 (**A**) and D_2O (**B**) and their fits to a Guinier-Porod model. Dimension parameters (s) and cross-sectional radii ($R_{g,cs}$) were as follows. DMSO-d_6: s=0.72 and $R_{g,cs}$=6.7 nm; D_2O: s=1.0 and $R_{g,cs}$=6.8 nm. Insets show power-law fits of **B2** in each solvent.

Brushes were transferred from a 1% wt solution in THF into an aqueous solution of THF (1:9 v^{THF}/v^{water}), to a final concentration of 0.1% wt using a multi-inlet vortex mixer (MIVM) to ensure rapid micromixing and homogenous precipitation.[52] SANS was carried out after dialyzing the resulting water/THF suspension against D_2O. Guinier-Porod analysis of the scattering profile in D_2O yielded a dimension parameter of s = 1.0 and $R_{g,cs}$ = 6.8 nm. The estimated brush radius in water was R = 9.6 nm, indicating that brush thickness is nearly unaffected by the change in solvent quality. As for the polymer in a selective solvent, the dependence of the form factor in the intermediate-q range was $1/Q^{1.2}$, ruling out the occurrence of a worm-to-sphere transition in the presence of a selective solvent for the PEG block (**Figure 2, B**). Molecular weights of the brush in DMF (6.5×10^6 Da) and in water (6.9×10^6 Da) were measured by static light scattering (**S5**), showing no appreciable change. This is indicative of primarily intramolecular collapse in water, wherein individual brushes are effectively stabilized by PEG side-chains. This is further supported by the scattering curve of the polymer in D_2O, which, compared to that in DMSO, also showed only a small difference in molecular weight on transfer to a purely aqueous environment.

Brushes were used to encapsulate rose bengal lactone (RBL) and probucol (PBC) as model hydrophobic solutes (**Table S1**). The former is a known potent inhibitor of kinesis and an effective sensitizer of singlet oxygen,[53, 54] while the latter is an antihyperlipidemic drug and a BCS class II model drug.[55, 56] Polymer and the corresponding solute were dissolved in THF; polymer concentration was maintained constant (10 mg/mL), while solute concentration was either 5% or 15% $w_{solute}/w_{polymer}$. The THF solution was fed into a four-inlet vortex mixer, along with three streams of water to achieve a final concentration of 10% v/v THF. Protocols for measuring drug loading capacity (DLC) and efficiency (DLE), and other details regarding loaded sample preparation, are provided in the Supporting Information.

The drug loading capacity and efficiency (DLC and DLE, respectively) of PBC at 5% and 15% w_{solute}/w_p solute feeds were $DLC^{(5\%)}$ = 3.6% and $DLE^{(5\%)}$ = 82.5%, and $DLC^{(15\%)}$ = 11.5% and $DLE^{(15\%)}$ = 95.5%, respectively. Similarly, for RBL $DLC^{(15\%)}$ = 11.8% and $DLE^{(15\%)}$ = 83.7%. These results show that **B2** is an effective stabilizer of both solutes, within the range examined. Molecular weight measurements of PBC-loaded particles by static light scattering revealed an increase in the molecular weight of loaded nanoparticles with respect to the molecular weight of the polymer in water of 1.3 × for a feed of 5% w/w_p, suggesting a combination of intramolecular collapse and intermolecular aggregation at this composition. This behavior was more pronounced as the solute content was raised to 15% w/w_p feed, resulting in a considerably larger increase (3.3 ×), clearly indicating the formation of multimolecular aggregates. While it was not possible to measure the weight average molecular weights of particles loaded with RBL by static light scattering, SANS provided important information to contrast the behavior of both solutes.

SANS profiles of PBC- and RBL-loaded particles are provided in **Figure 3**. Almost no change was observed for RBL-loaded particles with respect to the bottlebrush in D_2O, suggesting effective intramolecular stabilization at both concentrations of the solute. Guinier-Porod analysis of these samples yielded results similar to those observed for the polymer in water with a small increase in gyration radii (*i.e.*, brush radii), as shown in **Table S2**. Conversely, scattering from PBC-containing samples shows a strong departure from the polymer in D_2O. Differences in the low-q scattering range indicate an increase in molecular weight, the extent of which varies with solute concentration. This is consistent with the SLS data, which also showed that weight average molecular weights of PBC-loaded samples increased with solute feed. Guinier analysis of the intermediate-q region of 5% and 15% PBC-containing samples

showed a higher order dependence (>2, see **S6**), possibly resulting from brush stacking.

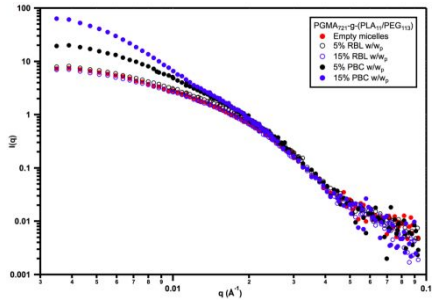

Figure 3. Small-angle neutron scattering profiles of PBC- and RBL-containing heterografted brushes at different solute concentrations (5 and 15% w/w_p). PBC samples are shown as filled symbols, whereas RBL samples are shown as open symbols. The scattering profile of **B2** in water is also provided as reference.

TEM images of RBL- and PBC-loaded particles (**Figure 4**) confirm that the worm-like morphology of the heterografted brush is preserved even for the highest drug:polymer ratio. Cryo-TEM images of PBC-containing particles also show the expected brush morphology but the increase in molecular weight observed by SANS or SLS cannot be distinguished using this method. In the case of RBL, the solute is expected to be localized inside the hydrophobic region formed by the (collapsed) backbone and PLA side-chains, stabilized by PEG. Single-molecule stabilization did not occur for PBC, according to SANS and SLS data, therefore we anticipate inter-brush interaction/stacking took place to stabilize PBC nanoparticles. In this context, the high mixing energy characteristic of the MIVM used is to promote micromixing so as to enhance polymer/solute co-localization during the change in solvent quality. Other experiments from our group had demonstrated the effects of mixing (batch vs. MIVM) on encapsulation and the morphologies of the resulting particles.[57]

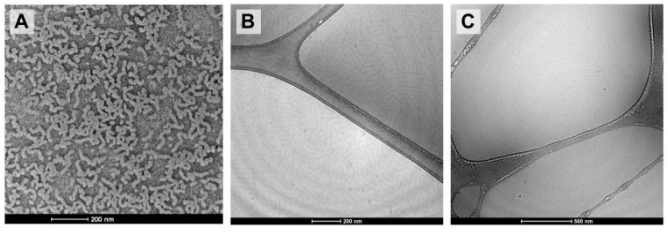

Figure 4. TEM and cryo-TEM images of RBL- and PBC-containing heterografted brushes at feed concentrations of 15% w/w_p. Images **(A)** and **(B)** correspond to RBL-loaded samples; **(C)** corresponds to a PBC-loaded sample. The worm-like morphology of the brushes demonstrates that grafting longer PEG chains from the backbone effectively prevents solute-induced morphological transitions of the polymer in the presence of either hydrophobic solute. Scale bars for images **A**, **B**, and **C** are 200 nm, 200 nm and 500 nm, respectively.

Overall, these results contrast with previously reported data from our group which showed that encapsulation of RBL and PBC by a heterografted brush with shorter PEG chains (2 kDa vs. 5 kDa) resulted in brush collapse into spherical particles at the concentrations here examined. It appears that grafting a longer PEG side-chain effectively prevents the worm-to-sphere transition resulting from solute-induced core compaction, highlighting the importance of side-chain properties on brush morphology. Nevertheless, solute-dependent differences exist even for longer side-chain bottlebrushes.

To examine the solute-dependent behavior observed for heterografted brushes, we studied PBC and RBL loading using a linear diblock copolymer (PEG_{113}-*b*-PLA_{125}), which self-assembles into well-defined spherical nanoparticles with a diameter of 32 nm. Encapsulation was achieved by imposing the same large and rapid change in solvent quality as for the heterografted brush, and solute feeds in the range of 5-100% w/w_p were examined. Average sizes and size distributions of loaded particles were measured by dynamic light scattering, and the results are presented in **Figure 5**.

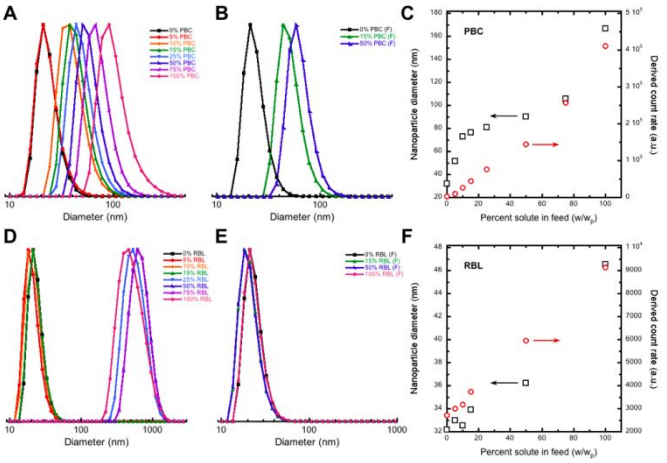

Figure 5. Dynamic light scattering results for PBC (**A** through **C**) and RBL (**D** through **F**) nanoparticles stabilized with PEG_{113}-*b*-PLA_{125}. The distributions shown in **A** and **D** (number distributions) correspond to unfiltered samples, whereas those presented in **B** and **E** correspond to samples filtered through 0.45 µm filters. **C** and **F** show particle diameters and their corresponding derived count rates as functions of feed concentration. Sizes and derived count rates of samples produced with feeds of 15%, 50% and 100% w/w_p correspond to filtered samples.

As observed, PBC-containing nanoparticles increase continuously in size with solute feed, following a trend similar to that previously observed for other hydrophobic solutes stabilized by linear amphiphilic diblock copolymers.[58, 59] Filtration of selected PBC samples through 0.45 µm filters had essentially no effect (~ 3% decrease) on particle size and derived count rate. Conversely, RBL nanoparticle diameters increased only very slightly (Δ ~ 2 nm) for feeds < 15% w/w_p but at higher feed ratios very large aggregates —with diameters exceeding 300 nm— were observed. Filtration removed the large aggregates, yielding considerably smaller particles. Similarly, the range of the derived count rate for PBC nanoparticles was considerably larger than for RBL due to the formation of larger particles (for PBC) and the removal of large aggregates (for RBL).

Drug loading capacity (DLC) and efficiency (DLE) were also measured for nanoparticles stabilized by the linear diblock copolymer. In the case of PBC, DLC increased with feed, as expected, whereas the DLE was relatively constant with a slight decrease at higher concentrations (**S7**). The DLC of RBL also increased with feed, however, the DLE, which was very high at low feeds, decreased more dramatically at higher RBL concentrations likely due to the removal of large aggregates on filtration. Comparatively, DLC and DLE values for the

heterografted brush were similar or higher than the corresponding results from the linear diblock, suggesting that the heterografted brush is equally if not a more effective stabilizer under these conditions. It is important, however, to realize that a direct comparison of these two systems is not straightforward as they differ in terms of their molecular architectures and weights, as well as their mechanisms of encapsulation —i.e., a balance of intra- vs. intermolecular association— all of which may influence their abilities as stabilizers.

Increasing particle size with solute concentration has been explained as an increase in the growth rate of the core relative to the rate of nucleation.[58, 60, 61] Stabilization by the linear diblock copolymer has been explained by the diffusion-limited aggregation of both the copolymer —through its hydrophobic component— and the supersaturated hydrophobic solute.[60, 61] As both solutes are present at high supersaturations, there are no nucleation barriers to assembly so the solute-dependent behavior observed here may be caused by solvent-mediated effects such as Ostwald ripening. Comparing particle sizes at low feeds (<25%), it appears that RBL forms more and smaller nuclei than PBC, since its nanoparticles were considerably smaller. The growth of larger particles at the extent of smaller ones would, therefore, be more likely to occur for RBL. Furthermore, RBL solubility in water is roughly 13 times higher than that of PBC, facilitating solvent-mediated effects. If RBL formed more, yet smaller nuclei, it may also explain why it could be effectively stabilized by the heterografted bottlebrush within the hydrophobic core formed by the PGMA backbone and PLA side-chains, with minimal modification to its structure and without intermolecular aggregation. The opposite behavior is expected for PBC; the larger PBC particles were poorly stabilized inside the hydrophobic region of single heterografted brushes, requiring highly entropic inter-brush interactions to occur.

Conclusions

In this work, we discussed the effect of side-chain length on the encapsulation properties of amphiphilic heterografted bottlebrushes. By grafting a long hydrophilic block to the double-brush, we were able to restrict solute-induced conformational changes, thus producing drug-loaded anisotropic carriers. Unimolecular encapsulation in brushes was not, however, solute-independent as shown here for RBL and PBC. Stabilization with an amphiphilic diblock copolymer —consisting of the same type of blocks as those comprising the heterografted brush— served to explain the solute-dependent behavior observed for brushes, suggesting that solutes with a higher propensity to nucleation could be more effectively stabilized by the anisotropic carrier in a unimolecular worm-like construct.

Conflicts of interest

There are no conflicts to declare.

Acknowledgements

We acknowledge financial support by the National Science Foundation (CMMI-1562639).

Notes and references

1 C. Kinnear, T. Moore, L. Rodriguez-Lorenzo, B. Rothen-Rutishauser and A. Petri-Fink, *Chem Rev*, 2017, **117**, 11476-11521.
2 R. A. Meyer and J. J. Green, *Journal*, 2016, **8**, 191-207.
3 J. C. Foster, S. Varlas, B. Couturaud, Z. Coe and R. K. O'Reilly, *J Am Chem Soc*, 2019, **141**, 2742-2753.
4 M. Elsabahy and K. L. Wooley, *Chem Soc Rev*, 2012, **41**, 2545-2561.
5 A. Albanese, P. S. Tang and W. C. W. Chan, *Annual Review of Biomedical Engineering*, 2012, **14**, 1-16.
6 A. Da Silva-Candal, T. Brown, V. Krishnan, I. Lopez-Loureiro, P. Ávila-Gómez, A. Pusuluri, A. Pérez-Díaz, C. Correa-Paz, P. Hervella, J. Castillo, S. Mitragotri and F. Campos, *Journal of Controlled Release*, 2019, **309**, 94-105.
7 G. Chen, Y. Wang, R. Xie and S. Gong, *Adv Drug Deliver Rev*, 2018, **130**, 58-72.
8 Z. Liu, Y. Huang, X. L. Zhang, X. Tu, M. Wang, L. Ma, B. Wang, J. He, P. Ni and H. Wei, *Macromolecules*, 2018, **51**, 7672-7679.
9 X. Y. Tu, C. Meng, X. L. Zhang, M. G. Jin, X. S. Zhang, X. Z. Zhao, Y. F. Wang, L. W. Ma, B. Y. Wang, M. Z. Liu and H. Wei, *Macromol. Biosci.*, 2018, **18**, n/a-n/a.
10 Y. Cheng, Q. Wu, Y. Li, J. Hu and T. Xu, *The journal of physical chemistry. B*, 2009, **113**, 8339.
11 W. Cao, J. Zhou, A. Mann, Y. Wang and L. Zhu, *Biomacromolecules*, 2011, **12**, 2697.
12 R. K. Kainthan and D. E. Brooks, *Bioconjugate Chem*, 2008, **19**, 2231.
13 Y. Lin, X. Liu, Z. Dong, B. Li, X. Chen and Y.-S. Li, *Biomacromolecules*, 2008, **9**, 2629.
14 O. G. Schramm, G. M. Pavlov, H. P. van Erp, M. A. R. Meier, R. Hoogenboom and U. S. Schubert, *Macromolecules*, 2009, **42**, 1808-1816.
15 K. Knop, D. Pretzel, A. Urbanek, T. Rudolph, D. H. Scharf, A. Schallon, M. Wagner, S. Schubert, M. Kiehntopf, A. A. Brakhage, F. H. Schacher and U. S. Schubert, *Biomacromolecules*, 2013, **14**, 2536.
16 T. Jia, S. Huang, C. Yang and M. Wang, *Mol Pharmaceut*, 2017, **14**, 2529.
17 X. Shi, M. Hou, S. Bai, X. Ma, Y.-E. Gao, B. Xiao, P. Xue, Y. Kang, Z. Xu and C. M. Li, *Mol Pharmaceut*, 2017, **14**, 4032.
18 J. Guo, H. Hong, G. Chen, S. Shi, T. R. Nayak, C. P. Theuer, T. E. Barnhart, W. Cai and S. Gong, *ACS Appl. Mater. Interfaces*, 2014, **6**, 21769-21779.
19 D. Chan, A. C. Yu and E. A. Appel, *Biomacromolecules*, 2017, **18**, 1434.
20 H. Y. Luo, M. Szymusiak, E. A. Garcia, L. L. Lock, H. G. Cui, Y. Liu and M. Herrera-Alonso, *Macromolecules*, 2017, **50**, 2201-2206.
21 H. Li, H. Liu, T. Nie, Y. Chen, Z. Wang, H. Huang, L. Liu and Y. Chen, *Biomaterials*, 2018, **178**, 620-629.
22 O. V. Borisov and E. B. Zhulina, *Macromolecules*, 2005, **38**, 2506-2514.
23 B. Parrish, R. B. Breitenkamp and T. Emrick, *Journal of the American Chemical Society*, 2005, **127**, 7404-7410.
24 R. B. Breitenkamp and T. Emrick, *Biomacromolecules*, 2008, **9**, 2495-2500.
25 E. Ostmark, D. Nystrom and E. Malmstrom, *Macromolecules*, 2008, **41**, 4405-4415.

26 M. R. Xie, J. Y. Dang, H. J. Han, W. Z. Wang, J. W. Liu, X. H. He and Y. Q. Zhang, *Macromolecules*, 2008, **41**, 9004-9010.
27 P. Kosovan, J. Kuldova, Z. Limpouchova, K. Prochazka, E. B. Zhulina and O. V. Borisov, *Macromolecules*, 2009, **42**, 6748-6760.
28 V. Vasilevskaya, P. G. Khalatur and A. Khokhlov, *Macromolecules*, 2003, **36**, 10103-10111.
29 V. V. Vasilevskaya, A. A. Klochkov, A. A. Lazutin, P. G. Khalatur and A. R. Khokhlov, *Macromolecules*, 2004, **37**, 5444-5460.
30 L. Gu, Z. Shen, S. Zhang, G. Lu, X. Zhang and X. Huang, *Macromolecules*, 2007, **40**, 4486-4493.
31 X. M. Lian, D. X. Wu, X. H. Song and H. Y. Zhao, *Macromolecules*, 2010, **43**, 7434-7445.
32 H. Chang, Y. Lin and Y. Sheng, *Macromolecules*, 2012, **45**, 4778-4789.
33 J. A. Johnson, Y. Y. Lu, A. O. Burts, Y. Xia, A. C. Durrell, D. A. Tirrell and R. H. Grubbs, *Macromolecules*, 2010, **43**, 10326-10335.
34 K. Huang, A. Jacobs and J. Rzayev, *Biomacromolecules*, 2011, **12**, 2327-2334.
35 Y. Yu, C. K. Chen, W. C. Law, J. Mok, J. Zou, P. N. Prasad and C. Cheng, *Mol Pharmaceut*, 2013, **10**, 867-874.
36 G. Chen, L. Wang, T. Cordie, C. Vokoun, K. W. Eliceiri and S. Gong, *Biomaterials*, 2015, **47**, 41-50.
37 V. Heroguez, Y. Gnanou and M. Fontanille, *Macromolecules*, 1997, **30**, 4791-4798.
38 L. N. Gu, Z. Shen, S. Zhang, G. L. Lu, X. H. Zhang and X. Y. Huang, *Macromolecules*, 2007, **40**, 4486-4493.
39 P. E. Theodorakis, W. Paul and K. Binder, *Macromolecules*, 2010, **43**, 5137-5148.
40 H. Y. Luo, J. L. Santos and M. Herrera-Alonso, *Chem Commun*, 2014, **50**, 536-538.
41 K. Ishizu, N. Sawada, J. Satoh and A. Sogabe, *J Mater Sci Lett*, 2003, **22**, 1219-1222.
42 Y. K. Li, L. Christian-Tabak, V. L. F. Fuan, J. Zou and C. Cheng, *J Polym Sci Pol Chem*, 2014, **52**, 3250-3259.
43 H. Li, H. Miao, Y. Gao, H. M. Li and D. Y. Chen, *Polym Chem-Uk*, 2016, **7**, 4476-4485.
44 B. Gumus, M. Herrera-Alonso and A. Ramrez-Hernndez, *Soft Matter*, 2020, **16**, 4969-4979.
45 P. Zhao, L. X. Liu, X. Q. Feng, C. Wang, X. T. Shuai and Y. M. Chen, *Macromol Rapid Comm*, 2012, **33**, 1351-1355.
46 Y. Chen, H. Zhou, Z. Sun, H. Li, H. Huang, L. Liu and Y. Chen, *Polymer*, 2018, **149**, 316-324.
47 B. Hammouda, Journal of Applied Crystallography, 2010, **43**, 716-719.
48 Y. Ruff, E. Buhler, S. J. Candau, E. Kesselman, Y. Talmon and J. M. Lehn, *J Am Chem Soc*, 2010, **132**, 2573-2584.
49 S. L. Pesek, X. Y. Li, B. Hammouda, K. L. Hong and R. Verduzco, *Macromolecules*, 2013, **46**, 6998-7005.
50 S. Rathgeber, T. Pakula, A. Wilk, K. Matyjaszewski and K. L. Beers, *Journal of Chemical Physics*, 2005, **122**.
51 D. Gromadzki, A. Jigounov, P. Stepanek and R. Makuska, *European Polymer Journal*, 2010, **46**, 804-813.
52 R. K. Prud'homme, Y. Liu, C. Y. Cheng, Y. Liu and R. O. Fox, *Chem Eng Sci*, 2008, **63**, 2829-2842.
53 S. C. Hopkins, R. D. Vale and I. D. Kuntz, *Biochemistry-Us*, 2000, **39**, 2805-2814.
54 L. D. Lu, F. H. Rininsland, S. K. Wittenburg, K. E. Achyuthan, D. W. McBranch and D. G. Whitten, *Langmuir*, 2005, **21**, 10154-10159.
55 M. C. Dalsin, S. Tale and T. M. Reineke, *Biomacromolecules*, 2014, **15**, 500-511.
56 J. M. Ting, T. S. Navale, F. S. Bates and T. M. Reineke, *Macromolecules*, 2014, **47**, 6554-6565.
57 H. Y. Luo, D. Raciti, C. Wang and M. Herrera-Alonso, *Mol Pharmaceut*, 2016, **13**, 1855-1865.
58 H. Shen, S. Y. Hong, R. K. Prud'homme and Y. Liu, *J Nanopart Res*, 2011, **13**, 4109-4120.
59 Z. Zhu, Mol Pharmaceut, 2014, **11**, 776.
60 S. M. D'Addio and R. K. Prud'homme, *Adv Drug Deliver Rev*, 2011, **63**, 417-426.
61 R. F. Pagels, J. Edelstein, C. Tang and R. K. Prud'homme, *Nano Lett*, 2018, **18**, 1139-1144.

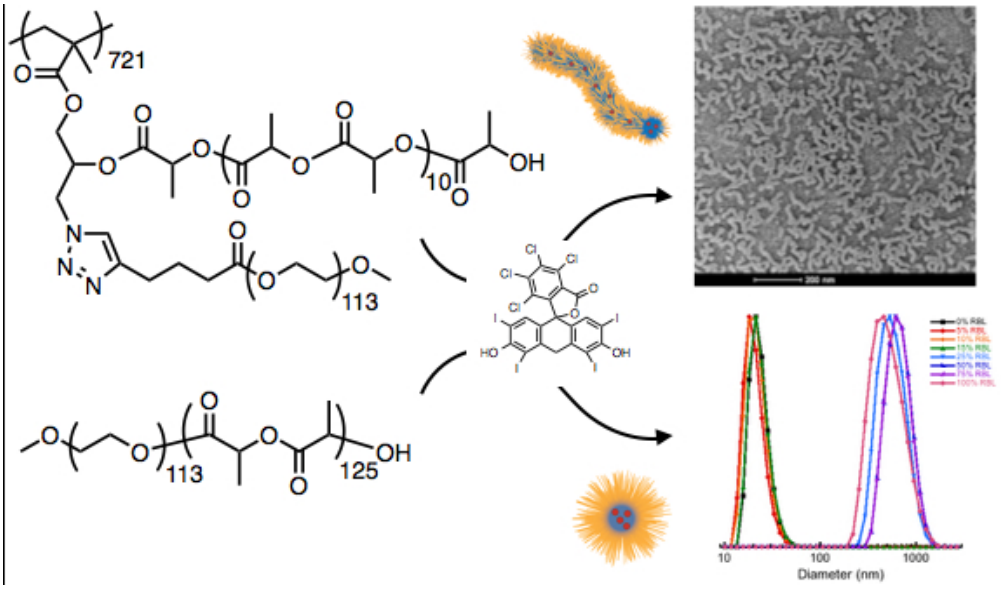

202x117mm (72 x 72 DPI)